Journal of Thermal Science Vol.34, No.3 (2025) 707–719

https://doi.org/10.1007/s11630-025-2106-5 **Article ID: 1003-2169(2025)03-0707-13**

Numerical Study of the Stagnation-Flow Premixed Lean Hydrogen/Air Flame Stabilized at the Wall with the Focus on NO Emission and Flame-Solid Interaction

Chunkan YU[1*], Cheng CHI[2], Chongchong TANG[3], Bronislava GORR[3]

1. Institute of Technical Thermodynamics, Karlsruhe Institute of Technology, Karlsruhe 76131, Germany
2. Lab. of Fluid Dynamics and Technical Flows, University of Magdeburg "Otto von Guericke", Magdeburg 39106, Germany
3. Institute for Applied Materials-Applied Materials Physics (IAM-AMP), Karlsruhe Institute of Technology, Karlsruhe 76131, Germany

Abstract: In this study, we perform a numerical investigation of a steady laminar stagnation flow flame stabilized at a wall with the consideration of heat transport, focusing on a lean hydrogen/air mixture with a fuel/air equivalence ratio 0.6. We discuss the NO emissions and their formation rates under various conditions, such as flow velocity and combustion pressure. It is found that the predominant reaction pathway for NO formation involves NNH radicals, though this changes near the wall surface. Beyond examining the wall's influence on flame structures, the present work focuses on the impact of combustion process on materials. Specifically, the accumulation of atomic hydrogen at the wall surface is explored, which is significant for the consequent modeling of potential hydrogen embrittlement. Additionally, the growth rate of oxide layers on the material surface increases significantly if the combustion pressure and consequently the combustion temperatures are enhanced. These investigations offer valuable insights into how combustion processes affect material, which is useful for designing engineering components under high-temperature environments.

Keywords: stagnation flow flame; hydrogen; NO_x emission; laminar premixed flame; strain rate

1. Introduction

Hydrogen combustion is gaining more and more attention since it is a clean energy source with the primary byproduct being water (H_2O). This makes hydrogen an attractive alternative to fossil fuels, which produce carbon monoxide (CO), soot, and other pollutants during and after combustion processes [1, 2]. However, NO_x emissions, which have significant environmental implications such as contributing to smog formation, acid rain, and adverse health effects [3], are also a byproduct of hydrogen combustion. While hydrogen combustion is generally cleaner than fossil fuels due to the absence of carbon dioxide emissions, it can still produce nitrogen oxides (NO_x) under high-temperature or high-pressure conditions [4–6]. Furthermore, hydrogen is highly flammable, with risks of flame flashback and pre-ignition. Thus, a methodology for hydrogen combustion under lean conditions is proposed. The major features of a lean hydrogen flame

Received: Aug 03, 2024
AE: CHEN Zheng

Corresponding author: Chunkan YU E-mail: chunkan.yu@kit.edu

include high flame speed, a low flammability limit, enhanced flame stability, and, especially, reduced NO_x emissions [7]. Moreover, the increased amount of air in the hydrogen/air mixture can also mitigate the risk of hot spots that could lead to pre-ignition and reduce potential explosion hazards [7]. A detailed review on lean hydrogen combustion can be found in, for example, Refs. [7–9], and its practical application is achieved in gas turbines [10, 11] and SI engines [12, 13].

Investigation into the lean hydrogen combustion process has been performed from various aspects over the last decades. For example, the potential hydrogen explosion of a lean hydrogen-air mixture in a tank was studied experimentally in Ref. [14], attempting to capture the influence of ignitor positions on the flame propagation direction and velocity, pressure changes, and the efficiency of consuming hydrogen. In Ref. [15], the thermo-diffusive and hydrodynamic instabilities of a lean hydrogen flame were studied experimentally, presenting the influence of flame instabilities on lean H_2-fueled spark-ignition engines. In Ref. [16], three-dimensional direct numerical simulation was performed to study the turbulence-chemistry interaction in lean premixed hydrogen combustion, examining the impact of the Karlovitz number on flame structures and NO_x emission. In Ref. [4], NO_x formation in lean premixed turbulent hydrogen/air flames was studied using DNS simulation. It is reported that for very lean hydrogen systems, the NO_x concentration is less than 1.0×10^{-5}. The controlling mechanism for this low NO_x concentration is attributed to the reaction pathway through nitrous oxide, while the conventional thermal NO_x pathway becomes insignificant due to the reduced flame temperature. The goal of using lean hydrogen combustion systems is to achieve low NO_x emissions, as the European Union sets limits of 2.4×10^{-5} for new gas-fired turbines and 3.7×10^{-5} for new oil-fired turbines.

Although lean combustion processes have been intensively studied, more issues may arise in real engineering applications when considering the interactions between the combustion process and materials. Among these there are, for example:

(1) Thermal stress and fatigue: The high temperatures associated with hydrogen combustion can cause thermal stress and fatigue in materials, potentially leading to cracks and failures over time [17, 18]. Therefore, during the combustion processes, knowledge about the thermal load and the temperature distribution inside the surrounding solid material is required.

(2) Hydrogen embrittlement: In the presence of hydrogen, the produced atomic hydrogen during combustion can diffuse into metals, and can cause serious degradation of metal mechanical properties such as ductility, toughness and fatigue resistance [19, 20]. Therefore, it is interesting to investigate the effect of combustion process on the concentration of atomic hydrogen at the wall surface, which may probably enter into a metal through surface physical adsorption for the next step [21, 22].

(3) High-temperature corrosion: During combustion process, the combined effects of high temperature, high pressure and the presence of reactive gases cause the solid surfaces of the combustion chamber or the interacted wall to corrode, forming an oxide layer. Unlike conventional carbon-contained fuels, hydrogen combustion produces a large amount of hot water vapor during combustion process [23, 24]. Depending on combustion conditions such as flow velocity or pressure, the resulting different wall surface temperatures and partial pressure of water vapor may significantly affect the type of oxide formation and its morphology, as well as the oxidation/corrosion kinetics [25, 26]. Understanding the relationship between combustion conditions and oxidation rate is also important for predicting material degradation and improving the durability of components exposed to hydrogen combustion environments.

The effects of the combustion process of various fuel on material performance have been studied in various literature. For example, in Ref. [27], the thermo-mechanical stress and fatigue life analysis of a diesel engine piston with oxy-fuel combustion was investigated based on a coupled CFD/FEM method. In Ref. [28], the selection of high-temperature materials was discussed and reviewed comprehensively. Moreover, the impact of ammonia combustion systems on material properties, selection, and design has been extensively reviewed in Ref. [29]. The study discussed the influence of the combustion system on aspects such as hydrogen embrittlement and corrosion effects. In Ref. [30], the effects of wall temperature and water vapor produced by ammonia combustion on the nitriding of stainless steel were investigated through both experimental and numerical methods, with the resulting changes in Vickers hardness reported.

The present work aims at studying the steady lean hydrogen/air flame interaction with a wall. The influence of heat conduction inside the wall is considered, and the effect of such heat loss on the flame structures and NO_x emissions will be discussed. Attention will also be paid to the atomic hydrogen accumulated at the wall surface to provide useful information about consequent hydrogen embrittlement. Moreover, since a large amount of water vapor will be produced during the combustion process and the wall surface will be subjected to high temperatures, the possible oxidation rate for the

formation of an oxide layer will also be investigated. Its variation under different combustion conditions (e.g., flow velocity, combustion pressures) will be represented.

2. Mathematical Model

2.1 Combustion configuration

Fig. 1 shows the schematic illustration of steady laminar stagnation flow flame. The coordinate has so chosen, that the computational domain for flame is in positive z-axis and the computational domain for solid wall in negative z-axis.

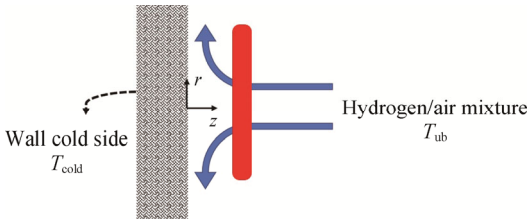

Fig. 1 Schematic illustration of steady laminar stagnation flow premixed hydrogen/air flame

The premixed unburnt mixture consists of fully mixed hydrogen and air with a temperature T_{ub}, and a premixed flame will be stabilized at the wall. Due to high flame temperature, heat will be lost through the wall at the position z=0, which is the interface between gas phase flame and solid phase wall. The other side of the wall has a lower temperature T_{cold}, and the convective heat transfer is neglected there. This corresponds to a fixed temperature set at this position (Dirichlet boundary condition). The existence of convective heat transfer on the cold side of the wall may further affect the surface temperature at the position z=0 [31].

The system is operated under isobaric condition over the whole domain, and the combustion pressure is given a-priori.

An important quantity describing the flame structure of a stagnation flow premixed flame is the strain rate imposed on the flow. This quantity is directly related to the outflow velocity: the higher the strain rate, the higher the outflow velocity. The governing equations used for the numerical simulation follow those proposed in Ref. [32], which include the tangential pressure gradient J. Subsequently, the strain rate a can be calculated as [32]

$$a = \sqrt{-J/\rho_{g,ub}} \tag{1}$$

where $\rho_{g,ub}$ is the mixture density of unburnt gas. More detailed description can be found in Ref. [32].

2.2 Gas mixture and chemical kinetic model

Lean hydrogen/air combustion systems are designed to operate with an excess of air, with a particular attraction for their potential to reduce emissions of nitrogen oxides (NO_x) [33]. The present work focuses on the lean premixed hydrogen/air mixture with the fuel/air equivalence ratio 0.6 as an example. The selection of this equivalence ratio is consistent with the one chosen in Ref. [4]. In that study, it was confirmed that at ambient pressure, the reaction pathway $N_2 \rightarrow N_2O$ becomes important under this condition. This aspect will therefore be reviewed for the stagnation flow premixed flame and extended to examine its validity at higher combustion pressures.

The chemical mechanism used for the present work consists of two parts: (1) the sub-mechanism for hydrogen/nitrogen/air system is from Ref. [34], which includes 9 species (H_2, O_2, N_2, H, O, OH, HO_2, H_2O_2, H_2O), and has been validated for various combustion systems such as explosion limits [34]. (2) the sub-mechanism for the N-H-O chemistry is from Ref. [5], which includes 21 species (NO, NO_2, NO_3, N_2O, HNO, HON, HONO, HNO_2, H_2NO, HNOH, $HONO_2$, NH_3, NH_2, NH, N, N_2H_4, N_2H_3, N_2H_2, H_2NN, NNH, NH_2OH).

Since NO emission, a primary emission in the hydrogen flame, will be investigated later, we will briefly outline several of the most important routes for NO formation at lean conditions. Readers can refer to Refs. [5, 6] for a more detailed discussion.

The route for thermal NO involves the elementary reaction $N_2 + O \Leftrightarrow NO + N$, which is strongly dependent on temperature. However, as pointed out in Ref. [4], for lean hydrogen/air flames, the flame temperatures are not sufficient high to support thermal NO formation.

The reaction pathway analysis in Refs. [4, 35] shows that at lean conditions, the NO formation through NNH radicals becomes predominant via the initiation step

$$NNH \Leftrightarrow N_2 + H .$$

The most important steps for the formation of NO via this NNH route are

$$NNH + O \Leftrightarrow NH + NO,\ NH + O \Leftrightarrow NO + H .$$

Another route for NO formation is through N_2O radicals via the reactions

$$N_2 + O(+M) \Leftrightarrow N_2O(+M),\ N_2O + O \Leftrightarrow NO + NO .$$

For this route, NO is promoted through N_2O at high pressures due to the presence of a third body M. However, as calculated in Ref. [4], N_2O radicals have only a minor impact on the formation of NO compared to NNH radicals.

Note that there are also other reaction pathways such as $N_2 \rightarrow NNH \rightarrow N_2H_2 \rightarrow N_2H_3 \rightarrow NH \rightarrow N \rightarrow NO$, which is proposed in Ref. [36]. However, the formation of NO via N_2H_3 radicals is of importance in rich hydrogen flames.

Furthermore, it should be pointed out that surface reactions are not included in the present work. In other words, the quenching of radical atoms at the metal wall

surface is not considered. However, the absorption of radical atoms at the wall surface may potentially alter their consumption and is the focus of our ongoing research.

2.3 Material selection and its corrosive behavior

Throuhgout the whole work, the Inconel 718 is selected as wall material. It is a high-strength, corrosion-resistant nickel-chromium based alloy, which is widely used in high-temperature engineering applications due to its excellent mechanical properties and resistance to oxidation and creep at high temperatures [37, 38]. To determine the temperature distribution inside the wall, its heat conductivity is required. According to Ref. [39], the Inconel 718 has the heat conductivity k in W/(m·K) as

$$k(T) = 7.69 + 0.0146T \tag{2}$$

Furthermore, due to its importance in thermal engineering applications, the high-temperature oxidation behavior of Inconel 718 in a dry atmosphere has been extensively studied, and its oxidation kinetics can be described by a parabolic law [40–42]. However, limited research exists on its oxidation behavior in water vapor-containing or pure steam atmospheres. A comparative analysis of its oxidation behavior in dry and water vapor-containing atmospheres revealed that the materials form the same type of oxide (a Cr_2O_3 scale) with comparable oxidation rates, although slightly higher rates were observed in the water vapor environment [43]. It should also be emphasized that oxidation of Inconel 718 in air with 10% H_2O resulted in net mass losses due to the formation of volatile $CrO_2(OH)_2$ at 700°C, while positive oxidation kinetics was recorded at 800°C. According to Ref. [43], the parabolic rate constant K_p (with unit $mg^2 \cdot cm^4/s$) in steam environment, describing the mass gain of oxide layer, can be fitted according to the Arrhenius relation as

$$K_p = K_p^0 \exp\left(-\frac{E_a}{RT}\right) \tag{3}$$

with parameters K_p^0 =0.0995 $mg^2 \cdot cm^4/s$ and E_a=137.57 kJ/(mol·K). The fitted parabolic rate constant against temperature together with the measured value from [43] is shown in Fig. 2, in which red error bars are measured.

2.4 Numerical simulation

The numerical simulation is carried out using the in-house INSFLA code [34] which has been validated against experimental measurements for various laminar flame configurations. To ensure efficient combustion simulation, an automatic adaptive meshing technique [34] is employed. This technique captures domains with high scalar gradients, where more grid points are necessary for accurate resolution. A more detailed description for the numerical simulation can be found in Ref. [44].

It should be mentioned here that the growth of the oxide layer is not included in the modeling, but only the value of the corrosion parabolic rate constant, which depends on the wall surface temperature, and is shown as an important indicator to describe the possible growth rate of the oxide layer.

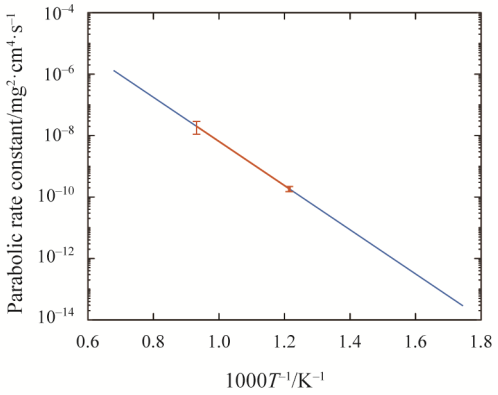

Fig. 2 Arrhenius plot of Inconel 718 parabolic rate constant versus temperature with the measurement from Ref. [43] (red error bar)

3. Results and Discussion at Pressure of 0.1 MPa

3.1 Temperature profile

Starting from the results, we show first in Fig. 3 the temperature profiles for flames imposed with three different strain rates at p=0.1 MPa and without considering the surface reaction. The wall, made from Inconel 718, has a thickness of d_w=10 mm.

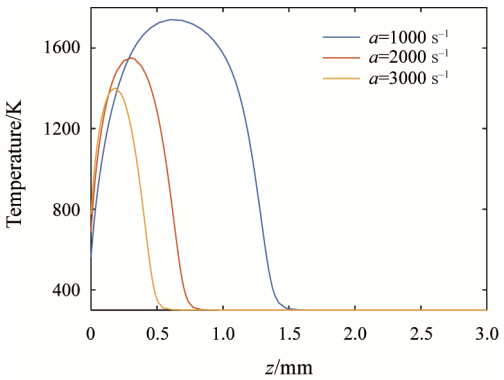

Fig. 3 Temperature profiles for flames imposed with three different strain rates. Combustion conditions: p=0.1 MPa, without surface reactions; Material: wall thickness d_w=10 mm, Inconel 718.

As the strain rate, indicating the flow velocity, becomes larger, the flame front approaches closer to the wall and the peak of flame temperature decreases due to

increasing convective molecular transport and a decreasing degree of complete reaction, as also reported previously in Refs. [45, 46]. However, although the flame temperature decreases with increasing strain rates, the wall is affected more by the flame due to (1) reduced distance between the wall and flame front, and (2) an increased temperature gradient at the wall surface since the flame becomes narrower with increasing strain rates. Both factors lead to an increase in wall surface temperature. This can be further observed in Fig. 4, where the temperature at the wall surface and peak flame temperature against strain rate are presented. The opposite tendencies for these two temperature quantities are clearly observed. For the shown example, the wall surface temperature increases from 560 K to 780 K when the corresponding strain rates are increased from 1000 s^{-1} to 3000 s^{-1}. However, the corresponding peak flame temperature decreases from 1720 K to 1350 K accordingly. Note that the rightmost point where the curves end corresponds to the extinction strain rate, beyond which no stable flame can be sustained. The mechanism controlling the extinction rate of hydrogen flames is discussed in detail elsewhere, for example, in Refs. [47, 48].

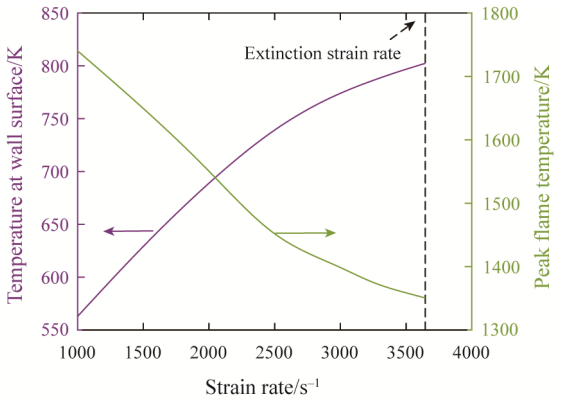

Fig. 4 Dependence of temperature at wall surface (purple line, left y axis) and peak flame temperature (green, right y axis) on the strain rate. Combustion conditions: p=0.1 MPa, without surface reactions; Material: wall thickness d_w=10 mm, Inconel 718.

3.2 Heat release rate

The heat release rate (HRR) is a measure of the rate of chemical energy released per unit time during the combustion process [13], which is defined as:

$$\mathrm{HRR} = \sum_{i=1}^{n_s} \dot{\omega}_i h_i \tag{4}$$

where $\dot{\omega}_i$ and h_i are the net production rate and enthalpy for species i, and n_s is the number of species.

In Fig. 5, we show the HRR profiles for flames imposed with three different strain rates. All conditions are the same as in Fig. 3. We see that if the flame is imposed with a low strain rate, causing the flame to be far away from the wall, the HRR at the wall is extremely low. As the strain rate becomes larger and the flame front approaches closer to the wall, the HRR at the wall surface increases significantly. At a very high strain rate (here a=3000 s^{-1}), the flame even has its HRR peak at the wall surface.

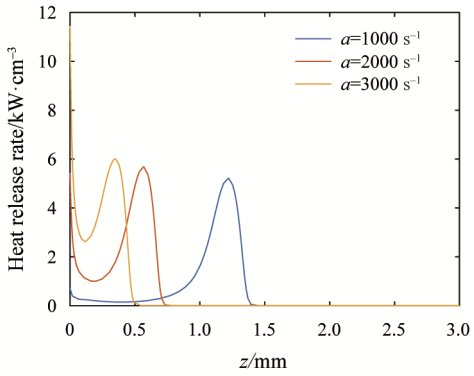

Fig. 5 Heat release rate profiles for flames imposed with three different strain rates. All conditions are the same as in Fig. 3.

To understand which reactions contribute significantly to the HRR at the wall surface, Fig. 6 presents the eight reactions that contribute most to HRR at the wall surface, under the same conditions as in Fig. 3. The most important contributor is the recombination reaction $\mathrm{H+O_2+M \Leftrightarrow HO_2+M}$, which is a highly exothermic process and leads to considerable heat release at the wall. The importance of this recombination reaction on the HRR at the cold wall has also been reported in Ref. [49].

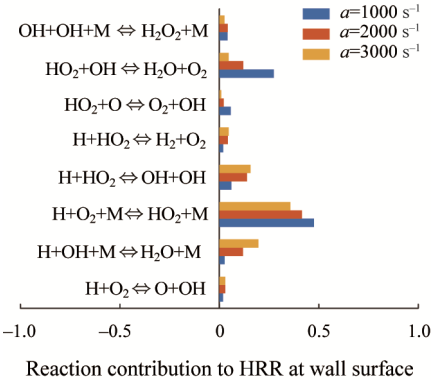

Fig. 6 The eight reactions contributing most to HRR at the wall surface. Blue, red and yellow bars represent different strain rates, as indicated in the legend. All conditions are the same as in Fig. 3.

Fig. 7 further shows the spatial distribution of the heat release rates of several key reactions for a flame imposed with a strain rate of a=3000 s^{-1}. It is clearly seen that the recombination reaction $\mathrm{H+O_2+M \Leftrightarrow HO_2+M}$ is the

most important reaction contributing to the HRR throughout the whole spatial domain. This reaction not only contributes the most at the wall surface but also significantly away from the wall. Interestingly, another recombination reaction, $H+OH+M \Leftrightarrow H_2O+M$, plays an important role in the HRR at the wall surface but decreases significantly farther from the wall surface.

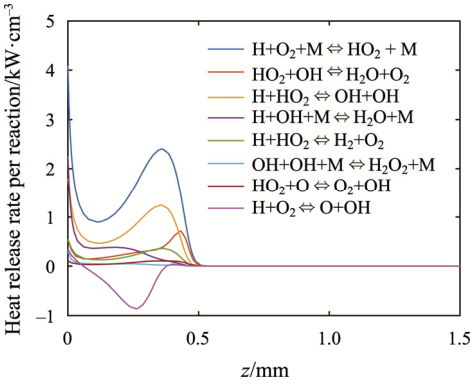

Fig. 7 Profiles of heat release rate per reaction for flames over space. Strain rate: a=3000 s^{-1}. All other conditions are the same as in Fig. 3.

3.3 Atomic hydrogen profile

Hydrogen embrittlement occurs in a hydrogen environment, which requires the presence of atomic hydrogen [50]. Therefore, in this section, the mole fraction of atomic hydrogen will be studied. Note that although the adsorption of atomic hydrogen at the wall surface is not modeled, this study still provides useful information on the maximum possible amount of atomic hydrogen that can be absorbed at the surface and enter the metal to cause hydrogen embrittlement.

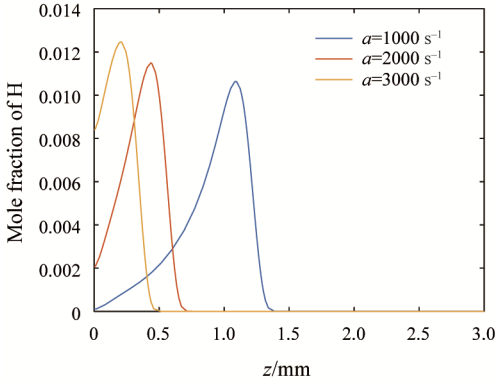

Fig. 8 Atomic hydrogen profiles for flames imposed with three different strain rates. All conditions are the same as in Fig. 3.

Fig. 8 represents atomic hydrogen profiles for flames imposed with three different strain rates. All conditions are the same as in Fig. 3. It is interesting to see that with increasing strain rates, more atomic hydrogen is accumulated at the wall surface. Fig. 9 (left y-axis) shows that the atomic hydrogen mole fraction at the wall surface increases with the strain rate, reaching a maximum of 1.2% under the highest strain rate just before flame extinction. This significant accumulation of atomic hydrogen at the wall surface is noteworthy. For context, as reported in Ref. [51], the Nickel-based alloy A725 can be degraded by a hydrogen surface concentration as low as 1.0×10^{-5}. Furthermore, for high-nitrogen stainless steel, hydrogen concentrations exceeding 2.0×10^{-3} can lead to a reduction in fracture elongation.

The accumulation of atomic hydrogen at the surface can primarily be explained by the increased flow convection. As the flame strain rate increases, the corresponding convective flow rate also increases, causing more atomic hydrogen to move toward the wall surface with the flow. Since there is a stagnation point at the wall surface, the increased flow rate results in a higher concentration gradient at and near the wall surface, which further enhances the physical and chemical processes controlling the accumulation of atomic hydrogen there. To understand this, we analyze the formation rate of atomic hydrogen as plotted in Fig. 9. It is noted that atomic hydrogen is actually consumed at the wall surface, indicated by the negative formation rate. Additionally, the consumption rate increases monotonically with increasing strain rate. This suggests that even though atomic hydrogen is being consumed at the wall surface, the supply from the flame reaction zone towards the wall due to diffusion is significant enough to result in a net accumulation. In other words, the increasing strain rate enhances the transport of atomic hydrogen to the wall, leading to higher diffusion flux towards the wall (c.f. positive concentration gradient at the wall surface in Fig. 8) and higher surface concentrations despite the consumption.

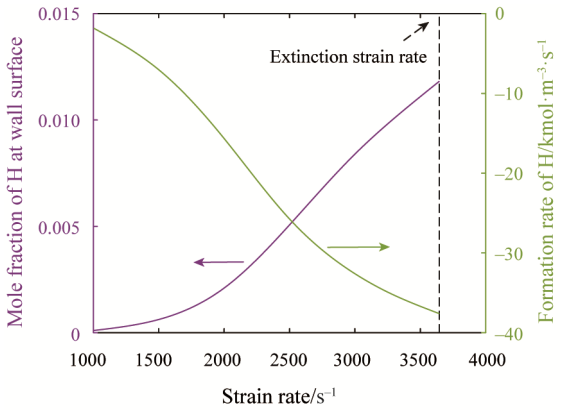

Fig. 9 Dependence of atomic H concentration at wall surface (purple line, left y axis) and atomic H formation rate (green, right y axis) on the strain rate. Combustion conditions: p=0.1 MPa, without surface reactions; Material: wall thickness d_w=10 mm, Inconel 718.

The remaining question is which reactions contribute primarily to the consumption of atomic hydrogen at the wall surface. Therefore, Fig. 10 compares quantitatively the atomic hydrogen formation pathways for three different strain rates, and the most important two reactions for the formation of H and the most important three reactions for the consumption of H are shown in this figure. It is observed that the most prominent pathways of atomic hydrogen consumption are via $H+O_2+M\rightarrow HO_2+M$ and $H+HO_2\rightarrow OH+OH$ for all strain rates. It is interesting to mention that these two reactions are also the strong exothermic reactions and the most important contributors to the heat release rate at the wall (c.f. Fig. 6).

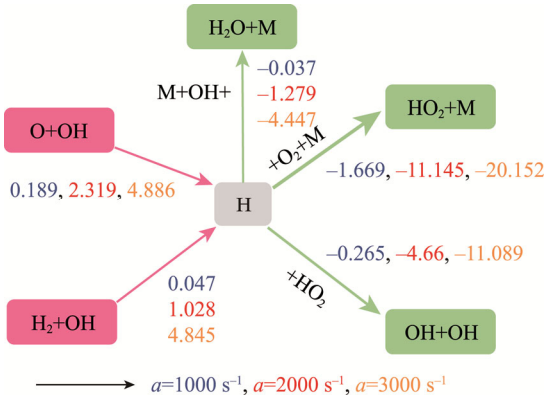

Fig. 10 Quantitative reaction path diagram showing H formation rate pathways at the wall surface. The value has the unit kmol/(m^3·s). All conditions are the same as in Fig. 3.

3.4 NO emission

The numerical results show that NO concentration (mole fraction) is at least two orders of magnitude higher than the NO_2 and N_2O concentrations. Therefore, in this section, we will focus solely on the NO concentration.

Fig. 11(a) shows the NO profile over the space domain for flames imposed with three different strain rates, under the same conditions as in Fig. 3. We observe that since the flame temperature is higher at low strain rates, the corresponding NO concentration is higher over the entire flame domain. Although the wall surface temperature is higher at high strain rates, this does not necessarily result in a higher NO concentration at the wall surface.

Taking a closer look at the NO formation rate, shown in Fig. 11(b), we observe that the peak NO formation rate occurs far from the wall, where high temperature regime is (c.f. Fig. 3), and the NO is formed (positive NO formation rate). Calculations show that for this position, around 45% of the NO is formed via $NNH+O\rightarrow NH+NO$, around 30% via $NH+O\rightarrow H+NO$ and around 20% via $N+OH\rightarrow H+NO$. Such observation is consistent with the one reported in Ref. [4] that at lean conditions the predominant reaction pathway to form NO is via NNH radicals.

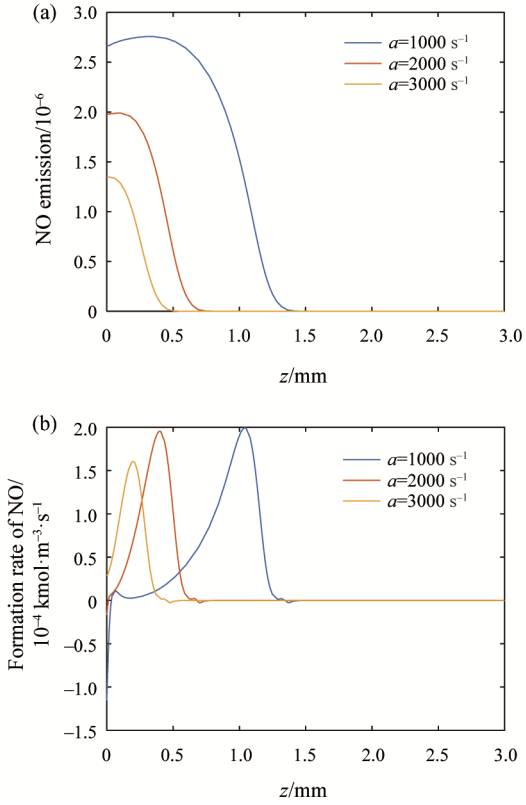

Fig. 11 (a) NO concentration profiles for flames imposed with three different strain rates. (b) Formation rate of NO profiles for flames imposed with three different strain rates. All conditions are the same as in Fig. 3.

However, it should be mainly emphasized here that the NO formation rates at the wall surface are not zero. Interestingly, the NO formation rates change from negative to positive as the strain rates increase. In other words, at low strain rates, NO is primarily consumed at the wall surface (indicated by a negative NO formation rate), whereas at high strain rates, NO is produced at the wall surface (indicated by a positive NO formation rate). To understand the chemical reason behind, Fig. 12 shows quantitative reaction path diagram for the NO formation rate pathways at the wall surface. In this diagram, the reaction $NO+HO_2\rightarrow NO_2+OH$ is the most significant step consuming almost 98% of the NO. However, it is noticeable that a large amount of NO at the wall surface is produced via the reaction $NO_2+H\rightarrow NO+OH$, which makes a minor contribution to the NO formation at its peak position. Indeed, at the wall surface with low temperatures (here 550 K–850 K, c.f. Fig. 4), NO participates in a rapid inter-conversion with NO_2 via the above-mentioned two reaction steps, which are the only significant reactions involving NO below approximately

1000 K. This is also observed and reported in Ref. [4]. If we read the quantitative values of the formation rate for both reactions, it is remarkable that the formation rate of NO through NO_2+H and the consumption rate of NO to NO_2 are approximately balanced with each other. The phenomenon that the NO formation rate at the wall surface switches from negative to positive as the strain rates increase is attributed to the fact that the wall surface temperature increases with increasing strain rate, so that NO can also be formed via N+OH→NO+H and NNH+O →NO+NH, which become faster at higher temperatures.

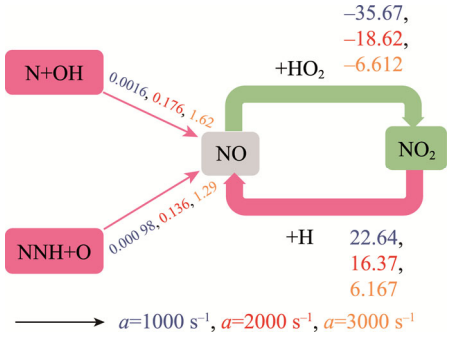

Fig. 12 Quantitative reaction path diagram showing NO formation rate pathways at the wall surface. The value has the unit 10^{-5} kmol/(m^3·s). All conditions are the same as in Fig. 3.

4. Results and Discussion at Higher Pressures

In this section, we will focus on the effect of varying pressure on the flame structure and the resulting oxidation rate of the oxide layer. The pressure varies from 0.1 MPa to 1.0 MPa, while the fuel/air equivalence ratio remains at Φ=0.6.

4.1 Temperature profile

Fig. 13 shows the temperature profiles for flames under three different pressures but with the same imposed strain rate (here a=9000 s^{-1} as an example). Two notable features of the impact of combustion pressure on the flame structure are: (1) the flame reaction zone becomes narrower and the temperature profile shows a higher gradient; and (2) the flame front moves closer to the wall due to reduced flame speed. Both of these features have also been reported earlier in other studies such as [52–54]. Due to these two factors, the wall surface becomes more affected by the flame, and the temperature gradient at the wall surface increases. Consequently, the temperature at the wall surface rises rapidly with increasing pressure.

An example in Fig. 14 shows in details the dependence of wall surface temperature on the combustion pressure if the flame is imposed with a high strain rate a=9000 s^{-1}. It is clearly observed that the wall surface temperature increases by approximately 220 K when the combustion pressure rises from 0.3 MPa to 1.0 MPa. Consequently, the resulting parabolic rate constant K_p can increase by one order of magnitude (see green line, right y-axis in Fig. 14). In other words, at elevated combustion pressures, the materials cope with exposure to more aggressive oxidizing conditions, resulting in a thicker and more rapidly growing oxide layer. The oxidation process becomes even more severe for flames imposed with higher strain rates, which lead to hotter wall surfaces.

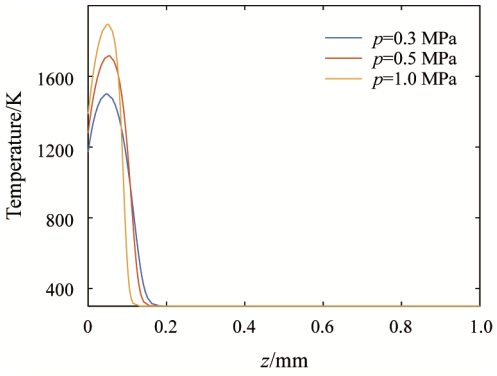

Fig. 13 Temperature profiles for flames under three different pressures. Flow condition: strain rate a=9000 s^{-1}; Combustion conditions: without surface reactions; Material: wall thickness d_w=10 mm, Inconel 718.

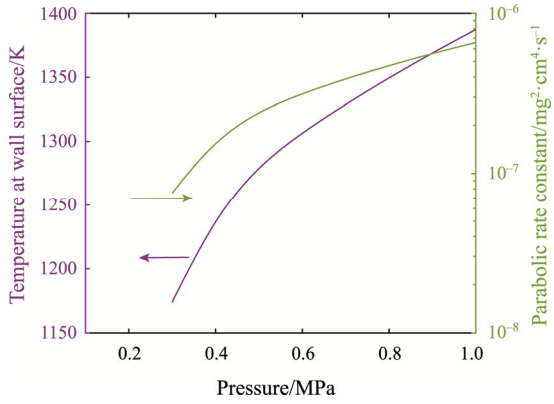

Fig. 14 Dependence of wall surface temperature (purple line, left y axis) and parabolic rate constant (green, right y axis) on the combustion pressure. Flow condition: strain rate a=9000 s^{-1}; Combustion conditions: without surface reactions; Material: wall thickness d_w=10 mm, Inconel 718.

4.2 Atomic hydrogen profile

As discussed in various studies [55, 56], hydrogen embrittlement increases with increasing gas pressure in gaseous hydrogen environments. As explained in Ref. [55], an increase in hydrogen pressure would increase the

chemical activity of hydrogen, so that a higher hydrogen concentration in the specimen is expected after the first crack is formed on the surface. Under the lean combustion process, hydrogen is normally consumed rapidly, and its concentration is even suppressed under high pressure. This can be observed in Fig. 15, where the atomic hydrogen profiles under three different combustion pressures are represented, and in Fig. 16, where the atomic hydrogen concentration at the wall surface and its corresponding formation rate over pressures are compared.

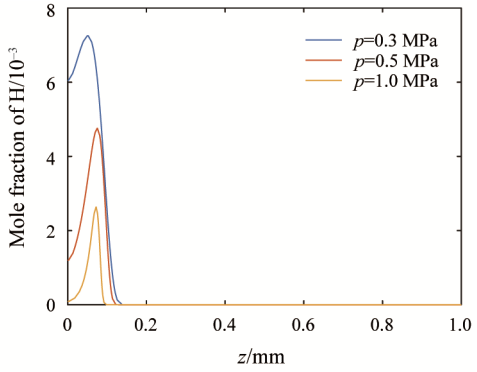

Fig. 15 Atomic hydrogen profiles for flames imposed with three different pressures. All conditions are the same as in Fig. 13.

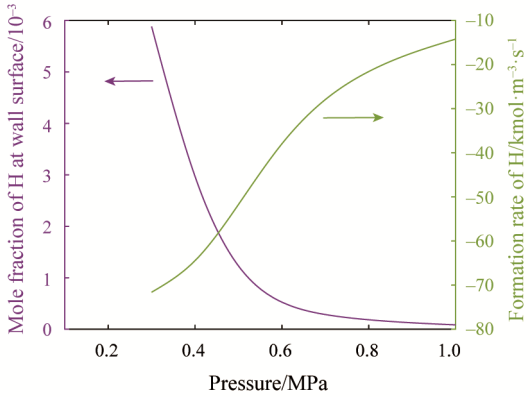

Fig. 16 Dependence of atomic H concentration at wall surface (purple line, left y axis) and atomic H formation rate (green, right y axis) on the combustion pressure. Combustion conditions: strain rate a=9000 s^{-1}; without surface reactions; Material: wall thickness d_w=10 mm, Inconel 718.

From the aspect of chemical kinetics, atomic hydrogen concentration decreases with increasing combustion pressure due to the chain termination step $H+O_2+M \rightarrow HO_2+M$, which is strongly pressure-dependent [34, 57]. This termination step consumes a large amount of atomic hydrogen, converting it to relatively stable HO_2. Therefore, high-pressure conditions result in reduced hydrogen concentration, including at the wall surface.

From the aspect of mass transport, the diffusion of atomic hydrogen becomes slower with increasing combustion pressure. Consequently, less atomic hydrogen will diffuse towards the wall surface and accumulate there. This results in a reduction of atomic hydrogen at the wall as well.

Based on these, it is concluded that for lean hydrogen/air system, higher combustion pressures can effectively reduce the risks associated with hydrogen-induced damage (e.g. hydrogen embrittlement and material degradation) by limiting the amount of atomic hydrogen that accumulates at the wall.

4.3 NO emission

Since increased combustion pressure raises both the flame temperature and the wall surface temperature, NO emissions are expected to vary at elevated pressures. Fig. 17(a) displays the NO concentration profiles for flames at three different pressures, with all conditions identical to those in Fig. 13. The corresponding formation rate of NO across the entire domain is shown in Fig. 17(b).

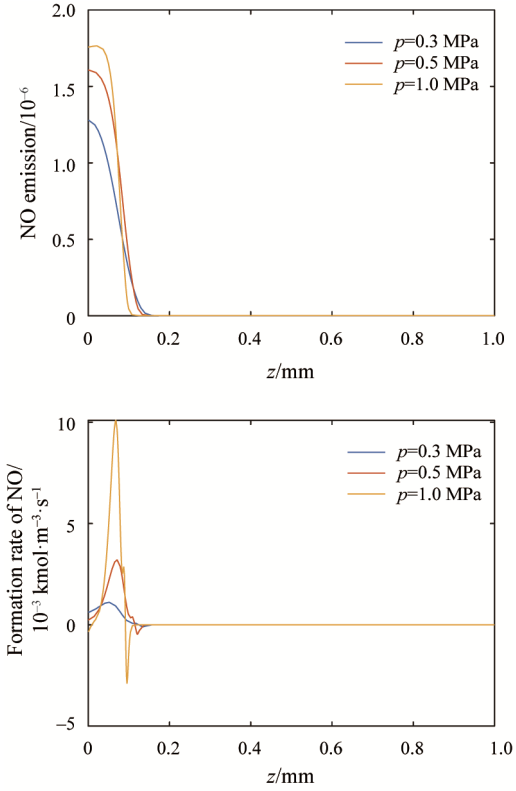

Fig. 17 (a) NO concentration profiles for flames imposed at three different pressures. (b) Formation rate of NO profiles for flames imposed with three different pressures. All conditions are the same as in Fig. 13.

It is clearly observed that the peak of the NO formation rate increases with increasing pressure, which can be explained by two reasons: (1) the predominant reaction NNH+O→NH+NO, which contributes the most to the formation of NO, becomes faster with increasing pressure, since the corresponding flame temperature increases (c.f. Fig. 13); and (2) the increase of combustion pressure enhances the reaction rate of N_2+O(+M)→N_2O(+M), which is pressure-dependent. The produced N_2O will further be used to produce NO, which is also reported in various other literature for NO emission at elevated pressure such as [36, 58, 59].

An interesting phenomenon is that while the NO concentration at the wall increases with increasing pressure, the corresponding NO formation rate at the wall decreases monotonically with increasing pressure. This is shown in Fig. 18, where flames are imposed with a strain rate of a=9000 s^{-1} as an example. It is clearly observed that the NO formation rate switches from positive to negative, indicating that with increasing pressure, the reaction steps consuming NO become significant. Reaction pathway analysis shows that at high pressure, the reaction step NO+HO_2→NO_2+OH contributes much more to the consumption of NO. This is because, at higher pressure, the pressure-dependent reaction H+O_2+M→HO_2+M becomes important in producing more HO_2, which is then used to support the reaction consuming NO.

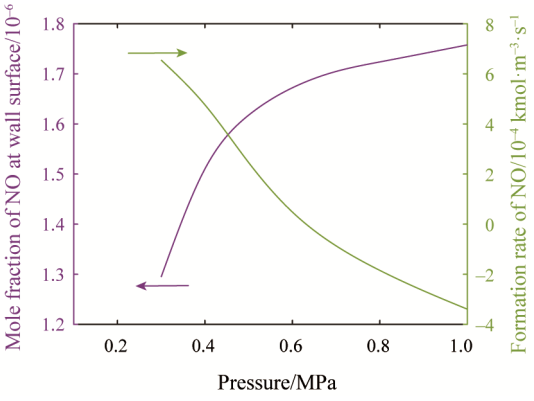

Fig. 18 Dependence of NO concentration at wall surface (purple line, left y axis) and NO formation rate (green, right y axis) on the combustion pressure. Combustion conditions: strain rate a=9000 s^{-1}; without surface reactions; Material: wall thickness d_w=10 mm, Inconel 718.

5. Conclusions

A numerical investigation on laminar, steady stagnation flow of a premixed lean hydrogen/air flame stabilized at a wall has been performed, focusing on the influence of wall heat loss on the flame structure. It is found that the increase in wall surface temperature can be attributed to either an increase in flame strain rate (causing the flame to move closer to the wall) or an increase in combustion pressure (causing the flame to become narrower and the temperature gradient to become larger). Due to the elevated wall surface temperature, the heat release rate (HRR) analysis shows that the peak HRR can exist at the wall surface. The recombination reaction $H + O_2 + M \Leftrightarrow HO_2 + M$ is identified as the most significant reaction contributing to the HRR at the wall surface. Additionally, the recombination reaction $H + OH + M \Leftrightarrow H_2O + M$ plays an important role in the HRR at the wall surface, but is much less significant farther from the wall.

Due to the elevated wall surface temperature and the production of water vapor as the main byproduct of hydrogen combustion, the experimentally determined parabolic oxidation rate constant obtained in the water vapor environment has been adopted to model the growth of the oxide layer on the material surface. It is found that increasing combustion pressure from 0.3 MPa to 1.0 MPa causes around 220 K enhancement of the wall surface temperature, which results in an increase by around one order of magnitude in the parabolic oxidation constant representative for the material corrosion resistance. The atomic hydrogen concentration at the wall surface is also investigated to understand the possible diffusion of hydrogen into the material, leading to consequent hydrogen embrittlement. For all considered conditions in the present work, the accumulation of atomic hydrogen at the wall surface is mainly attributed to the physical transport process. It is primarily consumed at the wall surface due to chemical reactions. The most prominent pathways for atomic hydrogen consumption are via H+O_2+M→HO_2+M and H+HO_2→OH+OH, which are also the most important contributors to the HRR at the wall.

The analysis of NO emissions reveals that different chemical reactions govern the reaction pathways of NO at its peak values and at the wall surface. At its peak value, most NO is produced via NNH radicals, and at high pressures partially via N_2O radicals due to the pressure-dependent reaction N_2+O(+M)→N_2O(+M). At the wall surface, NO participates in a rapid inter-conversion with NO_2 via NO+HO_2→NO_2 +OH and NO_2+H→NO+OH. At elevated pressures, the reaction step NO+HO_2→NO_2+OH becomes more significant due to increased HO_2 radicals via H+O_2+M→HO_2+M.

Acknowledgments

Chunkan YU acknowledges financial support by the DFG (project H2MAT3D, project number 523879740

within the DFG-SPP 2419 HyCAM). Cheng CHI would like to thank the Deutsche Forschungsgemeinschaft (DFG), Germany for its support within Project TH881/38-1 (DADOREN).

Conflict of Interest

On behalf of all authors, the corresponding author states that there is no conflict of interest.

Funding note

Open Access funding enabled and organized by Projekt DEAL.

Open Access

References

[1] Møller K.T., Jensen T.R., Akiba E., et al., Hydrogen-A sustainable energy carrier. Progress in Natural Science: Materials International, 2017, 27(1): 34–40.

[2] Dreizler A., Pitsch H., Scherer V., et al., The role of combustion science and technology in low and zero impact energy transformation processes. Applications in Energy and Combustion Science, 2021, 7: 100040.

[3] Sun Z., Wu Q., Zhao C., et al., A review of NO_x control by mild-oxy combustion. Journal of the Energy Institute, 2024, 113: 101502.

[4] Day M.S., Bell J.B., Gao X., et al., Numerical simulation of nitrogen oxide formation in lean premixed turbulent $H_2/O_2/N_2$ flames. Proceedings of the Combustion Institute, 2011, 33(1): 1591–1599.

[5] Mendiara T., Glarborg P., Ammonia chemistry in oxy-fuel combustion of methane. Combustion and Flame, 2009, 156(10): 1937–1949.

[6] Skottene M., Rian K.E., A study of NO_x formation in hydrogen flames. International Journal of Hydrogen Energy, 2007, 32(15): 3572–3585.

[7] Schefer R.W., White C., Keller J., Lean hydrogen combustion. Lean Combustion, Elsevier, 2008, pp. 213.

[8] Kumar V., Gupta D., Kumar N., Hydrogen use in internal combustion engine: A review. International Journal of Advanced Culture Technology, 2015, 3(2): 87–99.

[9] Du H., Chai W.S., Wei H., et al., Status and challenges for realizing low emission with hydrogen ultra-lean combustion. International Journal of Hydrogen Energy, 2024, 57: 1419–1436.

[10] Griebel P., Gas turbines and hydrogen. Hydrogen Science and Engineering: Materials, Processes, Systems and Technology, 2016, pp: 1011–1032.

[11] Marek C., Smith T., Kundu K., Low emission hydrogen combustors for gas turbines using lean direct injection. 41st AIAA/ASME/SAE/ASEE Joint Propulsion Conference & Exhibit, 2005, Paper No. AIAA 2005-3776.

[12] Kumar M.S., Muniyappan M., Selvan, S.A., Experimental and CFD analysis on the impact of hydrogen as fuel on the behavior of a passenger car gasoline direct injection engine. Journal of the Energy Institute, 2024, 113: 101487.

[13] Alvarez C.E.C., Couto G.E., Roso V.R., et al., A review of prechamber ignition systems as lean combustion technology for SI engines. Applied Thermal Engineering, 2018, 128: 107–120.

[14] Hu P., Zhai S., Experimental study of lean hydrogen-air mixture combustion in a 12 m^3 tank. Progress in Nuclear Energy, 2021, 133: 103633.

[15] Welch C., Erhard J., Shi H., et al., An experimental investigation of lean hydrogen flame instabilities in spark-ignition engines. Proceedings of the Combustion Institute, 2024, 40(1–4): 105391.

[16] Aspden A., Day M., Bell J., Turbulence-chemistry interaction in lean premixed hydrogen combustion. Proceedings of the Combustion Institute, 2015, 35(2): 1321–1329.

[17] Trabold C., Puck A., Gallas T., et al., Influence of hydrogen combustion on engine components in full load operation. Internationaler Motorenkongress, Springer, 2024, pp. 117–129.

[18] Stefan E., Talic B., Larring Y., et al., Materials challenges in hydrogen-fuelled gas turbines. International Materials Reviews, 2022, 67(5): 461–486.

[19] Djukic M.B., Zeravcic V.S., Bakic G.M., et al., Hydrogen damage of steels: A case study and hydrogen embrittlement model. Engineering Failure Analysis, 2015, 58: 485–498.

[20] Sun B., Zhao H., Dong X., et al., Current challenges in the utilization of hydrogen energy-a focused review on the issue of hydrogen-induced damage and embrittlement. Advances in Applied Energy, 2024, 14: 100168.

[21] Hasan M.S., Kapci M.F., Bal B., et al., An atomistic study on the help mechanism of hydrogen embrittlement in pure metal Fe. International Journal of Hydrogen Energy, 2024, 57: 60–68.

[22] Röthig M., Hoschke J., Tapia C., et al., A review of gas phase inhibition of gaseous hydrogen embrittlement in pipeline steels. International Journal of Hydrogen Energy, 2024, 60: 1239–1265.

[23] Jin Q., Dai G., Wang Y., et al., High-temperature corrosion of water-wall tubes in oxy-combustion atmosphere. Journal of the Energy Institute, 2020, 93(4): 1305–1312.

[24] Zhang T., Fetzer R., Heinzel A., et al., Corrosion behavior of various conductive materials in Sb_3Sn_7 alloy at 450°C. Corrosion Science, 2024, 227: 111797.

[25] Wright I.G., Dooley R., A review of the oxidation behaviour of structural alloys in steam. International Materials Reviews, 2010, 55(3): 129–167.

[26] Saunders S., Monteiro M., Rizzo F., The oxidation behaviour of metals and alloys at high temperatures in atmospheres containing water vapour: A review. Progress in materials science, 2008, 53(5): 775–837.

[27] Ugraram R., Reddy B., Reddy R.M., Thermo-mechanical stress and fatigue life analysis of diesel engine piston with oxy-fuel combustion and comparison with conventional air combustion. AIP Conference Proceedings, 2023, 2869(1): 040001.

[28] Pierce D., Haynes A., Hughes J., et al., High temperature materials for heavy duty diesel engines: Historical and future trends. Progress in Materials Science, 2019, 103: 109–179.

[29] Alnaeli M., Alnajideen M., Navaratne R., et al., High-temperature materials for complex components in ammonia/hydrogen gas turbines: A critical review. Energies, 2023, 16(19): 6973.

[30] Wang D., Xing Y., Lee M., et al., Effects of wall temperature and water vapor on the nitriding of stainless steel induced by ammonia flames. Proceedings of the Combustion Institute, 2024, 40(1–4): 105562.

[31] Xu S.T., Tu Y.J., Huang P., et al., Effects of wall temperature on methane MILD combustion and heat transfer behaviors with non-preheated air. Applied Thermal Engineering, 2020, 174: 115282.

[32] Stahl G., Warnatz J., Numerical investigation of time-dependent properties and extinction of strained methane- and propane-air flamelets. Combustion and Flame, 1991, 85(3–4): 285–299.

[33] Dunn-Rankin D., Lean combustion: Technology and control. Academic Press, 2011.

[34] Maas U., Warnatz J., Ignition processes in hydrogen-oxygen mixtures. Combustion and Flame, 1988, 74(1): 53–69.

[35] Capurso T., Laera D., Riber E., et al., NO_x pathways in lean partially premixed swirling H_2-air turbulent flame. Combustion and Flame, 2023, 248: 112581.

[36] Konnov A., Colson G., De Ruyck J., No formation rates for hydrogen combustion in stirred reactors. Fuel, 2001, 80(1): 49–65.

[37] Hosseini E., Popovich V., A review of mechanical properties of additively manufactured Inconel 718. Additive Manufacturing, 2019, 30: 100877.

[38] Sonar T., Balasubramanian V., Malarvizhi S., et al., An overview on welding of Inconel 718 alloy-effect of welding processes on microstructural evolution and mechanical properties of joints. Materials Characterization, 2021, 174: 110997.

[39] Woo W.-S., Lee C.-M., A study of the machining characteristics of AISI 1045 steel and Inconel 718 with a cylindrical shape in laser-assisted milling. Applied Thermal Engineering, 2015, 91: 33–42.

[40] Bataillou L., Martinelli L., Desgranges C., et al., Growth kinetics and characterization of chromia scales formed on Ni-30Cr alloy in impure argon at 700°C. Oxidation of Metals, 2020, 93: 329–353.

[41] Greene G., Finfrock C., Oxidation of Inconel 718 in air at high temperatures. Oxidation of Metals, 2001, 55: 505–521.

[42] Nnaji R., Bodude M., Osoba L., et al., Study on high-temperature oxidation kinetics of Haynes 282 and Inconel 718 nickel-based superalloys. The International Journal of Advanced Manufacturing Technology, 2020, 106: 1149–1160.

[43] Unocic K.A., Pint B., Effect of environment on the high temperature oxidation behavior of 718 and 718plus. In: 8th International Symposium on Superalloy 718 and Derivatives, 2014, pp. 667–677.

[44] Yu C., Böhlke T., Valera-Medina A., et al., Flame-solid interaction: Thermomechanical analysis for a steady laminar stagnation flow stoichiometric NH_3-H_2 flame at a plane wall. Energy & Fuels, 2023, 37(4): 3294–3306.

[45] Law C.K., Sung C., Yu G., et al., On the structural sensitivity of purely strained planar premixed flames to strain rate variations. Combustion and Flame, 1994, 98(1–2): 139–154.

[46] Egolfopoulos F.N., Zhang H., Zhang Z., Wall effects on the propagation and extinction of steady, strained, laminar premixed flames. Combustion and Flame, 1997, 109(1–2): 237–252.

[47] Jeon J., Shin D., Choi W., et al., Identification of the extinction mechanism of lean limit hydrogen flames

based on Lewis number effect. International Journal of Heat and Mass Transfer, 2021, 174: 121288.

[48] Fernández-Galisteo D., Sánchez A., Liñán A., et al., The hydrogen-air burning rate near the lean flammability limit. Combustion Theory and Modelling, 2009, 13(4): 741–761.

[49] Dabireau F., Cuenot B., Vermorel O., et al., Interaction of flames of H_2+O_2 with inert walls. Combustion and Flame, 2003, 135(1–2): 123–133.

[50] Dwivedi S.K., Vishwakarma M., Hydrogen embrittlement in different materials: A review. International Journal of Hydrogen Energy, 2018, 43(46): 21603–21616.

[51] Omura T., Nakamura J., Hirata H., et al., Effect of surface hydrogen concentration on hydrogen embrittlement properties of stainless steels and Ni based alloys. ISIJ International, 2016, 56(3): 405–412.

[52] Sohn C., Jeong I., Chung S., Numerical study of the effects of pressure and air-dilution on NO formation in laminar counterflow diffusion flames of methane in high temperature air. Combustion and Flame, 2002, 130(1–2): 83–93.

[53] Niemann U., Seshadri K., Williams F.A., Methane, ethane, and ethylene laminar counterflow diffusion flames at elevated pressures: Experimental and computational investigations up to 2.0 MPa. Combustion and Flame, 2014, 161(1): 138–146.

[54] Deng S., Han D., Law C.K., Ignition and extinction of strained nonpremixed cool flames at elevated pressures. Combustion and Flame, 2017, 176: 143–150.

[55] Nanninga N., Levy Y., Drexler E.S., et al., Comparison of hydrogen embrittlement in three pipeline steels in high pressure gaseous hydrogen environments. Corrosion Science, 2012, 59: 1–9.

[56] Michler T., Yukhimchuk A.A., Naumann J., Hydrogen environment embrittlement testing at low temperatures and high pressures. Corrosion Science, 2008, 50(12): 3519–3526.

[57] Wang X., Law C.K., An analysis of the explosion limits of hydrogen-oxygen mixtures. The Journal of Chemical Physics, 2013, 138(13): 134305.

[58] Xu S., Xi L., Tian S., et al., Numerical investigation of pressure and H_2O dilution effects on no formation and reduction pathways in pure hydrogen mild combustion. Applied Energy, 2023, 350: 121736.

[59] Frassoldati A., Faravelli T., Ranzi E., A wide range modeling study of NO_x formation and nitrogen chemistry in hydrogen combustion. International Journal of Hydrogen Energy, 2006, 31(15): 2310–2328.